TSUNAMI GENERATION BY SUBMARINE MASS FAILURE
PART II: CASE STUDIES

By Philip Watts[1], Stéphan T. Grilli[2], Member, ASCE, David R. Tappin[3], Gerard J. Fryer[4], and Loren W. Kroenke[4]

[1]Applied Fluids Engineering, Private Mail Box #237, 5710 E. 7th Street, Long Beach, CA 90803.
[2]Prof., Dept. of Oc. Engrg., Univ. of Rhode Island, Narragansett, RI 02882.
[3]Geologist, British Geological Survey, Keyworth, Nottingham, NG12 5GG, UK
[4]Prof., Hawaii Inst. of Geophys. and Planet., Univ. of Hawaii, Honolulu, HI 96822.

ABSTRACT:

We show that initial acceleration is the primary desriptor of center of mass motion during tsunami generation. We demonstrate that finite underwater landslide width will reduce characteristic tsunami amplitude. We solve an apparent paradox in slump center of mass motion whereby the distance traveled is proportional to the shear strength. We demonstrate that rundown and runup can be scaled with the characteristic tsunami amplitude. Our case studies of five potential landslide tsunamis show that our scaling and characteristic analyses can reproduce known tsunami amplitudes. We anticipate that the characteristic tsunami amplitude is a reasonable representation of maximum runup in a three-dimensional geometry. We therefore propose the Correspondence Principle as a logical extension of the case studies presented here.

INTRODUCTION

We developed theoretical equations in Part I of this work that we apply to actual case studies here. Before we can do so, we further our approximate and order of magnitude analyses in order to develop a complete range of analytical tools. With these additional tools, we aim to demonstrate the utility of our techniques rather than to claim their accuracy. We expect more accurate versions of our analyses and tools to appear as research progresses. Nevertheless, when we carry out the case studies, we will describe tsunami features that seem remarkably accurate in those instances when data are available for comparison. The choice between frictionless, translational slides and cohesive, rotational slumps requires a local geological context. Because of the considerable differences in tsunami features of slides and slumps, regional geology controls tsunami features generated by submarine mass failures (Watts, 2001). We surmise that tsunami source (or geological event) characterization is the single most important research activity related to landslide tsunamis. For example, marine cruises have been essential to identify the source of the 1998 Papua New Guinea tsunami as a slump instead of a slide (Tappin *et al.*, 1999, 2001). Marine geology research appears to afford important tsunami source information (Watts, 2001).

Underwater Landslide Geology

Tsunamis may be generated by coseismic sea floor displacement, submarine mass failure, volcanic activity, gas hydrate phase change, and oceanic meteor strikes. Submarine mass failure generation remains one of the least studied of these five mechanisms, in part because their occurrence is often concealed from view and in part because of the complicated dynamics involved in failure, center of mass motion, deformation, and tsunami generation (see Part I). Submarine mass failures pose difficulties for tsunami warning systems as they often occur on coastal margins near shorelines, can not be predicted as of yet, and may strike within minutes following a moderate earthquake. Local tsunami amplitude depends on at least four nondimensional geometric parameters (length, width, thickness, and inclination) that cannot be easily detected nor accurately predicted. On the other hand, tsunamis generated by submarine mass failure often cause limited damage outside of some local impact radius and one far-field azimuth (Plafker *et al.*, 1969; Iwasaki, 1997; Watts *et al.*, 2000). Submarine mass failures threaten coastal communities and economic activity throughout the Pacific Basin.

Submarine mass failure or underwater landslide are broad terms that encompasses reef failure, submarine rock slides, underwater slides, and underwater slumps (Schwab *et al.*, 1993). There are no clear definitions of these terms: rock may be significantly weathered, and sediment may be only partially lithified, sands and silts may possess cohesion, and cohesive muds may contain some sand and silt. These materials are often found to coexist in stratified layers of varying strength. The spectrum of mass failure materials yields a spectrum in modes of failure and subsequent behaviors. Likewise, there are often multiple failure mechanisms acting at once, such as increased pore water pressures combined with ground acceleration from a nearby earthquake (Hampton *et al.*, 1996). It may be fundamentally impossible to attribute submarine mass failure to any single mechanism. Most important, any submerged geological structure can be expected to undergo some degree of mass failure due to ground motion from a nearby earthquake (Kramer, 1996). As such, many forms of submarine mass failure can be present at the same time and may even trigger one another (Bjerrum, 1971; Tappin *et al.*, 1999, 2001). A reasonably strong earthquake can trigger thousands of landslides, whether subaerial or submarine (Wilson and Keefer, 1985; Watts, 2001). Given the ubiquity of submarine mass failure, we are indeed fortunate that most events are not tsunamigenic on account of either small length scales or deep submergence (Watts and Borrero, 2002).

Tsunamigenic underwater slides and slumps involve the failure of a mass of sediment that can range in length over more than six orders of magnitude, with larger events typically occurring less frequently (Prior and Coleman, 1979; Edgers and Karlsrud, 1982; Schwab *et al.*, 1993). Damaging tsunamis may result from the failure of sediment along steep fjords banks, near boundaries of submarine canyon systems, at active river deltas, along volcanic islands or ridges, or at submerged alluvial plains including continental margins (Hampton *et al.*, 1996). Terzaghi (1956) showed that underwater slides and slumps can often be related to excess pore water pressures along (at least) the initial failure plane. Prior and Coleman (1979) attribute excess pore water pressure to low tides, artesian water sources, recent external loads, rapid sedimentation, seismic ground motions, construction induced vibrations, volcanic activity, vaporization of gas hydrates, wave action, or any combination of these or similar factors. Hampton *et al.* (1996) separate these factors into those that reduce effective sediment strength and those that increase sediment stress. Sediment failure may occur spontaneously such as during extremely low tides; or, sediment failure may be triggered by a deterministic external agent such as ground motion during an earthquake (Kramer, 1996). The timing of spontaneous slides and slumps may be fundamentally unpredictable since failure of metastable sediments may precipitate from localized inhomogeneities of unknown weaknesses. A majority of tsunamigenic underwater slides and slumps appear to be triggered by nearby earthquakes.

Slide and Slump Similarities

Underwater slide and slump center of mass motions have similar functional forms $s/s_o = f(t/t_o)$, despite very different dynamics, because both represent accelerating bodies characterized by one length scale s_o and one time scale t_o. Equations of motion that contain one inertial term, one gravitational forcing term, and one retarding term are guaranteed unique length and time scales (Watts, 1997). This simplification of landslide motion is also the basis for our mechanical distinction of slides and slumps: by choosing one dominant retarding force (fluid dynamic drag *versus* basal friction), unique characteristics of motion are guaranteed. These underwater slide and slump center of mass motions are end members of a continuous spectrum of potential landslide motions. However, a center of mass motion that combines both basal friction and fluid dynamic drag would have two time scales of motion (Watts, 1997). If the two forces are of similar importance, then the two time scales will be of similar duration. Hence, tsunami generation by an underwater landslide with dynamics between those of an ideal slide and an ideal slump is more difficult to describe analytically, including through scaling analyses.

There are more specific similarities between slide and slump motion. The first terms in the Taylor series expansions about $t = 0$ are both $s(t) \approx a_o t^2/2$. The second terms have values of about 16% for slides and 8% for slumps of the first term, respectively, when evaluated at $t = t_o$. We thus find that the slide and slump motions during tsunami generation for $t < t_o$ are almost exclusively governed by the initial acceleration a_o. Conversely, we find that t_o is a general measure of the duration of acceleration. Given that $a_o = s_o/t_o^2$, we can write these "accelerational" motions as $s(t) = s_o(t/t_o)^2/2$ up until around $t \approx t_o$, at which time $s \approx 0.5s_o$. [The exact value of the coefficient is 0.43 for slides and 0.46 for slumps.] According to analyses of numerical simulation results, almost all tsunami generation occurs during times $t < t_o$. We have therefore proven that the salient center of mass motion experienced during tsunami generation is acceleration, and almost exclusively the initial acceleration (Tuck and Hwang, 1972). These observations justify the definitions of $0.5s_o$ and t_o as the distance and duration of acceleration, respectively, for both slides and slumps.

Our curve fits of tsunami amplitude in Part I obscure the role that initial acceleration plays in tsunami generation because that role remains implicit. We also acknowledge that the tsunami amplitude curve fits offer a level of detail that may be excessive when an order of magnitude tsunami amplitude is sought. Therefore, we offer a much simpler alternative to predict tsunami amplitude with the proviso that errors will be significantly larger. We begin by noting that Watts (2000) solved for a free surface response to landslide acceleration at very early times in the form

$$\eta(t) \approx - \frac{k\, a_o t^2 \sin\theta}{2} \tag{1}$$

where k represents the geometrical contribution to the tsunami amplitude (viz., d/b, θ, T/b), and the asymptotic approximation breaks down by growing indefinitely. By evaluating Eq. (1) after the duration of tsunami generation $t = t_o$, and accepting the gross approximation involved, we derive a characteristic tsunami amplitude $\eta_{2d} \approx 0.5 k s_o \sin\theta$, in full agreement with the scaling analysis of Watts (1998) and the idea that tsunami amplitude is proportional to vertical landslide displacement (Murty, 1979). The results from our simulations in Part I indicate that k = 0.005-0.030 over the range of underwater slides studied, and k = 0.02-0.30 over the range of underwater slumps studied. There is no point in seeking more precise values for the parameter k, because we would effectively be deriving new tsunami amplitude curve fits. These results show that slumps are (an order of magnitude) more efficient tsunami sources than slides when normalized by their characteristic distance of motion.

Landslide Tsunami Hazards

Coseismic displacement and submarine mass failure constitute the two most common forms of tsunami generation. Coseismic displacement, or vertical seafloor deformation, occurs during nearshore earthquakes and often generates tsunamis with longer wavelengths, longer periods, and a larger source area than those generated by submarine mass failures

(Hammack, 1973; Watts, 1998, 2000). Coseismic displacement generates tsunami amplitudes that correlate with earthquake magnitude (Hammack, 1973; Geist, 1998); submarine mass failures produce tsunamis with amplitudes limited only by the vertical extent of center of mass motion (Murty, 1979; Watts, 1998). These differences help identify the roughly 30% of Pacific Basin tsunamis that involve landslide tsunami amplitudes greater than the earthquake tsunami amplitude (Watts and Borrero, 2002). Landslide tsunamis therefore pose one of the greatest tsunami hazards to coastal population and infrastructure.

PRACTICAL DEVELOPMENTS

In Part I of this work, we developed tsunami amplitude equations that require several parameters to describe tsunami generation. These parameters are not necessarily commonly available from current research and they will often not be available prior to or immediately following an event. We therefore study some of these parameters in more detail with the hope of finding general scaling relations, or constraints on their expected ranges. During our analyses, we describe the impact of landslide width on three-dimensional tsunami generation. We finish this section with an examination of tsunami rundown and runup at the shoreline immediately behind mass failure.

Slump Radius of Curvature

Slump center of mass motion involves a radius of curvature R that can be difficult to reconstruct from bathymetry data and difficult to measure from seismic reflection data. A pragmatic means of estimating the radius of curvature is offered here based on a geometrical approximation of the failure surface. The failure surface is assumed to be a parabolic arc of linear length b and maximum depth T. Solving analytically for the radius of curvature yields

$$R = \frac{b^2}{8\,T} \tag{2}$$

where b and T are the same measures of landslide size used to estimate tsunami amplitude. By using (2), slump geometry is brought one step closer to the simpler geometry of a slide by writing the radius of curvature R as a function of more basic and observable length scales.

Slump Angular Displacement

With an approximate expression for the radius of curvature R, we turn our attention to approximations of the angular displacement $\Delta\phi$ of slumps. The angular displacement can be found from either i) the linear distance traveled by the slump, or ii) an estimate of the mean shear strength along the slump failure plane. Given a specific distance traveled by a slump center of mass

$$2\,s_o = R\,\Delta\phi \tag{3}$$

then either the radius of curvature R or the angular displacement $\Delta\phi$ is an independent quantity. Since the radius of curvature R faces geometrical constraints such as (2), it follows that the angular displacement $\Delta\phi$ can be viewed as a dependent quantity determined by the radius of curvature R and the distance traveled by the slump $2s_o$. On the other hand, if the distance traveled is not known, then the solution of the center of mass motion provides

$$\Delta\phi = \frac{8\,S_u}{\pi\,(\rho_b - \rho_o)\,T\,g} \tag{4}$$

which depends on an estimate of the mean shear strength S_u. Note that this shear strength is both a spatial and a temporal average as it covers the entire failure plane during the entire slump motion. Conversely, if the distance traveled by the center of mass is known, then Eqs. (3) and (4) can be combined to yield a characteristic shear strength S_u along the failure plane.

It is convenient to seek an approximate shear strength that can be used in conjunction with Eq. (4). Many normally consolidated marine sediments conform to the shear strength relation

$$S_u(z) \approx 0.3 \, (\rho_b - \rho_o) \, g \, z \tag{5}$$

where z is the local depth of the failure plane (Bardet, 1997). Assuming a linearly increasing shear strength with depth, a parabolic failure plane shape, and a thickness to length ratio $T/b \ll 1$, we find from integration along the arc length that the peak shear strength is approximately 60% larger than the mean shear strength. Therefore, the mean shear strength becomes

$$S_u \approx 0.19 \, (\rho_b - \rho_o) \, T \, g \tag{6}$$

where we have divided Eq. (5) by 1.6 and set $z = T$ to the maximum slump thickness. By substituting this expression for S_u into Eq. (4), the numerator and denominator of (4) both contain the scale $(\rho_b - \rho_o) \, T \, g$. This fact eliminates the paradox mentioned in Part I of this work that larger shear strengths increase the distance of slump motion as one might conclude from inspection of only Eq. (4).

When we substitute (6) into (4), we obtain a constant slump angular displacement of $\Delta\phi =$ 0.48 radians, or about 27˚. Because one can approximate $R \approx b$ (see below), it then follows directly from (3) that a typical slump travels roughly 50% of its length. However, Eq. (6) cannot be used to describe slump motion whenever the slump headwall coincides with a tectonic control fault. In such cases, failure may be induced by pressurized water within the fault pushing the sediment apart (Sibson, 1981; Tappin *et al.*, 2001; Martel, 2002). When this happens, the mean shear strength S_u can be expected to be considerably less than the value indicated by (6) because of the temporary presence of pressurized water along the failure plane. If (6) were uniformly valid, then all slumps would have the same angular displacement. Local variations in sediment composition can vary the shear strength coefficient in (6) by at least a factor of two (Bardet, 1997). However, some underwater slumps only achieve values around $\Delta\phi = 0.1$ radians, or advance 10% of their length (von Huene *et al.*, 2002). Such motion is unlikely to be explained solely by remolding of presumably low sensitivity sediment along the failure plane (Bardet, 1997). Other factors, such as water injection along the failure plane, are assumed to be lowering the apparent shear strength of the sediment. Therefore, we find that the angular displacement $\Delta\phi$ is in fact a measure of the departure of the characteristic shear strength from (6).

Thickness to Length Ratios

Landslide tsunamis can be inferred from nearshore data such as local runup maxima or time of arrival (Tappin *et al.*, 1999, 2001). Occassionally, underwater cable breaks, hydrophone records, or eyewitness observations provide direct evidence of mass failure (Bjerrum, 1971; Murty, 1979; Kulikov, 1996; Caplan-Auerbach, 2001). The tsunami amplitude estimates developed in Part I require knowledge of landslide dimensions that are not usually available immediately following an event. A method is required to estimate tsunamigenic potential before detailed marine surveys can be conducted, and perhaps even to motivate and direct such surveys. The initial landslide length b and mean depth d are often dictated by bathymetry and can sometimes be inferred from tsunami period or wavelength information. We now show that a typical underwater landslide thickness T can be estimated with an appeal to the geometries of documented underwater slides and slumps. Underwater slides typically exhibit maximum thickness to initial length ratios T/b of 0.5-2%; in contrast, underwater slumps often involve deep failure with maximum thickness to initial length ratios T/b of 5-15% (Prior and Coleman, 1979; Edgers and Karlsrud, 1982; Turner and Schuster, 1996). If a thin slide is a suspected tsunami source, for whatever reason, then a typical thickness

$$T \approx 0.01\, b \tag{7}$$

can be expected. On the other hand, if a cohesive slump is a suspected tsunami source, then a typical thickness

$$T \approx 0.10\, b \tag{8}$$

can be expected. Substituting (8) into (2) yields a typical radius of curvature $R \approx 1.3\, b$ for a slump. In general, the radius of curvature R can be expected to be 1-2 times the slump length b. We note that use of either (7) or (8) may introduce errors on the order of 100% into a tsunami amplitude calculation. At the same time, a choice between (7) or (8) alters the tsunami amplitude by an order of magnitude, demonstrating significant geometrical differences between slides and slumps. Schwab *et al.* (1993) estimate that nearly half of all mass failures off of the continental United States appear to satisfy translational sliding, while the other half appear to satisfy rotational slumping. The distinction is best made from local geological and sedimentary considerations whenever such data is available.

Nevertheless, the observed tsunami features can sometimes provide sufficient distinction to choose one landslide model over another.

The Effect of Landslide Width

Up until now, tsunami amplitude calculations have been based on the assumption of 2D mass failures. The 2D criteria may be met by less than half of all tsunamigenic submarine mass failures and so must be evaluated. For landslides of finite width, tsunami propagation in the third spatial dimension will reduce the two-dimensional tsunami amplitude. We follow the analytical developments of Watts *et al*. (2002a). Let an underwater landslide have a parabolic transverse profile of width w and maximum thickness T. In the absence of transverse propagation and with a uniform landslide length, the tsunami width would also be w and the transverse profile would also be parabolic. The cross-sectional area of displaced water is readily calculated as 2/3 of the maximum amplitude multiplied by the width. During the times $t < t_o$ of wave generation, the tsunami width will increase to approximately $w + \lambda_o$ due to transverse propagation, where λ_o is the characteristic wavelength. Transverse propagation will produce a wave form not dissimilar to $\mathrm{sech}^2(3y/(w+\lambda_o))$ with a maximum at $y = 0$ and exponentially decreasing leading edges as y becomes large (Mei, 1983). The numerical factor of three in the numerator is chosen to reduce the wave amplitude to 1% of its maximum amplitude at the transverse distance $y = w + \lambda_o$. The reduction in tsunami amplitude is found from conservation of mass (or cross-sectional area), as in the scaling work of Hammack (1973) and Watts (1998). We find that the two-dimensional characteristic tsunami amplitude is reduced by a factor

$$\frac{\eta_{3d}}{\eta_{2d}} = \frac{w}{(w + \lambda_o)} \qquad (9)$$

at $y = 0$ due to transverse propagation. The meaning of one of the two-dimensional criteria given in Part I is now clear: as the failure width w becomes much larger than the characteristic wavelength λ_o, the maximum tsunami amplitude becomes unaffected by transverse propagation. On the other hand, as the failure width w drops below the characteristic wavelength λ_o, the maximum tsunami amplitude is readily reduced by up to an order of magnitude or more. Eq. (9) possesses the correct behavior and scaling to convert two-dimensional tsunami maxima into three-dimensional tsunami maxima.

The preceding analysis demonstrates the importance of landslide width on a 3D measure of tsunami amplitude. We therefore seek approximate expressions for the width of slides and slumps. Underwater slides are often relatively narrow when compared with their length and tend to satisfy

$$w \approx 0.25\, b \tag{10}$$

according to Schwab *et al*. (1993), McAdoo *et al*. (2000), Syvitski and Hutton (2002), and von Huene *et al*. (2002). The reduction in amplitude depends on the water depth and cannot be computed in advance. Underwater slumps often have a width that is comparable to their length such that

$$w \approx 1.00\, b \tag{11}$$

according to Schwab *et al*. (1993), McAdoo *et al*. (2000), Tappin *et al*. (2001), and von Huene *et al*. (2002). It should be apparent by now that most underwater landslide physical dimensions can be scaled by the landslide length as a first approximation. There is no reason to assume that such relations will be universally valid. However, in the absence of better information, an estimate of tsunami amplitude in an order of magnitude sense remains possible. Watts *et al*. (2002b) show that it is reasonable, as a first approximation, to assume that mass failure occurs along the entire slope in question.

Tsunami Rundown and Runup

Our analyses have so far focused on a single measure of tsunami amplitude above underwater landslides. The historical origin of this characteristic tsunami amplitude lies in its simplicity to calculate and to measure (Pelinovsky and Poplavsky, 1996; Watts, 1997). The power behind this choice lies in the ability to relate this chosen characteristic tsunami amplitude to other measures of wave activity, such as the far-field Airy wave amplitude (Watts, 2000). Here, we relate the characteristic tsunami amplitude to the vertical rundown and runup of the leading depression wave arriving at the shoreline immediately behind the landslide. By curve fitting all of our numerical experiments in Part I for both slides and slumps, we find a minimum rundown

$$R_{min} \approx 1.25\eta_{2d} \tag{12}$$

where R is not to be confused with the radius of curvature. We also find a maximum runup

$$R_{max} \approx 0.27\eta_{2d} \tag{13}$$

where R^2 = 0.83 for both curve fits. The minimum rundown is greater than the characteristic tsunami amplitude. The maximum runup is comparable in amplitude to the far-field Airy wave studied by Watts (2000), where the coefficient is 0.30 instead of 0.27 in (13). Both rundown and runup results demonstrate that significant tsunami energy propagates back towards shore. This fact contradicts the depth-averaged results of Jiang and LeBlond (1992) and Tinti and Bortolucci (2000), calling into question once again the relevance of depth averaging to landslide tsunami generation (Watts *et al.*, 2000).

The 2D results in Eqs. (12) and (13) do not include bathymetric focusing of tsunamis, which can increase maximum runup 3-4 fold (Matsuyama *et al.*, 1999). Consequently, the characteristic tsunami amplitude can be a reasonable representation of maximum runup in a three-dimensional geometry by multiplying (13) by three or four. When we combine these results with the energy directionality described by Iwasaki (1997), we find that landslide tsunamis radiate energy along the axis of failure, with (13) representing a strong "recoil" of the water waves propagating in the direction of mass failure. The numerical coefficients in (12) and (13) are mild functions of incline angle and initial landslide depth, because the runup process includes shoreline interactions not taken into account by the characteristic tsunami amplitude. Therefore, we could formulate more sophisticated curve fits of maximum runup in the form $R_{max}/\eta_{2d} = \mathrm{f}(\theta, d/b)$ if we so desired. We present the simple curve fits (12) and (13) merely to refute claims that we have not examined nearshore or onshore tsunami phenomena. Instead, we confirm that the characteristic tsunami amplitude remains a fundamental and viable measure of tsunami amplitude from generation to propagation to runup.

UNDERWATER LANDSLIDE CASE STUDIES

The preceding equations have been applied successfully to a range of underwater slide and slump events in the course of their development. Here, the emphasis will be to demonstrate the utility of the analytical expressions rather than produce detailed computer simulations. Very few tsunami events with suspected mass failure tsunami generation have the necessary data even to employ these simple equations, let alone produce reliable simulations. Underwater slide motion is characterized by specific density γ, length along the incline b, and incline angle θ. These quantities can be estimated from bathymetry data acquired during a marine survey of suspected tsunami sources. Underwater slumps require a radius of curvature R, slump thickness T, and shear strength S_u to describe motion. These quantities require more sophisticated seismic reflection and core sampling tools. In either case, marine surveys conducted by experienced geologists are essential for understanding tsunamis generated by mass failure (e.g., Tappin *et al.*, 1999, 2001). Case studies are presented more or less in order of increasing uncertainty and speculation.

The 1998 Papua New Guinea Tsunami

The amplitude, time of arrival, and longshore distribution of the 10 m wave(s) that struck Sissano Lagoon are incommensurate with the epicentral location and magnitude ($M_w \approx 7$) of the main shock (Kawata *et al.*, 1999; Tappin *et al.*, 1999). In basic terms, any wave generated by the main shock appears to have been too small and too early to relate to eyewitness accounts. Marine surveys and seismic records point to a large submarine mass failure around twelve minutes after the main shock along the southern edge of an arcuate amphitheater (Watts *et al.*, 2002a). Sediment piston cores, remotely operated vehicle dives, and manned submersible dives confirm the presence of stiff marine clays deposited along a sediment starved margin (Tappin *et al.*, 2001). Seismic reflection surveys confirmed a $T =$ 760 m deep and $b = 4.5$ km long displaced mass that traveled approximately $2s_o = 670$ m along the failure plane (Sweet and Silver, 2002). With a ratio $T/b = 0.17$ and the presence of stiff clays, the tsunami was apparently created by an underwater slump that advanced only 15% of its length. We therefore seek two further physical parameters of the slump. First of all, Eq. (2) provides a radius of curvature $R = 3.3$ km that agrees reasonably well with the seismic reflection data of Sweet and Silver (2002). Second, the angular displacement $\Delta\phi = 0.23$ radians follows from (3). This angular displacement is at least two times less than expected for a continental margin covered by stiff clay, which may suggest the involvement of pressurized water in mass failure (Tappin *et al.*, 2001). The slump width is between 3-5 km, so we employ the value $w = 4.5$ km suggested by (11) until more precise data become available. The initial depth at the middle of the slump is around $d \approx 1.2$ km and the mean incline angle of the amphitheater nearby the slump is around $\theta = 12°$. We assume a typical specific density of marine sediment $\gamma = 1.85$ in order to complete the physical description of our case study.

Estimates of slump motion are necessary to characterize tsunami generation. We calculate an initial acceleration $a_o \approx 0.34$ m/s^2, a maximum velocity $u_{max} \approx 11$ m/s, a characteristic distance of motion $s_o \approx 335$ m, and a characteristic time of motion $t_o \approx 34$ s. The characteristic time of motion yields a characteristic wavelength $\lambda_o \approx 3.7$ km. The ratio $\lambda_o/d = 3.05 > 1$ ensures that the tsunami period is proportional to the characteristic time of motion, which will be true of all case studies made here. Near the region of tsunami generation, the wave propagates in a manner between deep water waves and shallow water waves (Watts, 2000). Given this intermediate wave behavior, far-field tsunami propagation begins at a radial distance r = 3-11 km from the source assuming constant depth d (Watts, 2000). We now check the applicability of our tsunami amplitude equation to this case study. The ratio $d/b = 0.27$ is sufficiently large to yield accurate results, yet sufficiently small to suggest weakly nonlinear tsunami generation (Watts, 1998). The value of $R/b = 0.74$ is less than unity, but this extrapolation will incur little error given the small power of this ratio governing tsunami generation. All other tsunami generation parameters are within their respective ranges for the curve fits. For this event, we find the tsunami amplitude ratio $w/(w+\lambda_o) = 0.55$ from (9) and a 3D characteristic tsunami amplitude above the slump of $\eta_{3d} \approx 11.7$ m which is similar to the maximum runup above sea level measured between 10-15 m in front of Sissano Lagoon (Kawata *et al.*, 1999). The Ursell parameter for this tsunami in an open ocean with $h = 4$ km is approximately $U = \eta_{3d}\ \lambda_o{}^2 / h^3 \approx 0.0024$ which indicates linear, dispersive wave propagation at this depth (Mei, 1983; Watts, 2000).

Our analyses therefore show that this catastrophic tsunami may be attributed to a single submarine mass failure.

Marine survey data and mechanical analyses afford us some geological insight into this event. Solving for the mean shear strength from (4) gives S_u = 590 kPa over the entire failure surface. This shear stress is about two times less than the expected value $S_u \approx 1.25$ MPa found from (6) despite the slump occurring in stiff clay. The fact that failure occurred about ten minutes after the main shock indicates that ground motion was not directly responsible for the slump. The presence of stiff clays also rules out significant pore fluid diffusion over such a relatively short time scale. There is however a suspected control fault running along and beneath the headwall of the slump that may have contributed to mass failure (Tappin *et al.*, 2001). A control fault can advect pressurized water (generated by the stress changes following the earthquake) into a position that can facilitate mass failure (Sibson, 1981; Martel, 2002). Our marine geology interpretation combined with the mean shear strength calculated here may indicate just such a mechanism. The slump volume $V \approx$ 6 km^3 had an average vertical drop of about 430 m (Sweet and Silver, 2002) that yielded a potential energy release of around 2.3×10^{16} J. This corresponds to a moment magnitude M_w = 7.7 earthquake if all of the potential energy were to go into a single elastic rupture. Two strong aftershocks occurred roughly 20 minutes after the main shock and in the same vicinity as the slump (Tappin *et al.*, 2001). These aftershocks may have been induced by the shift in overburden (Watts *et al.*, 2002a). Seismic activity shortly *after* tsunami generation may bolster the submarine mass failure hypothesis (Watts, 2001).

The 1994 Skagway, Alaska Tsunami

On Nov. 3, 1994, a partially aerial landslide in Skagway, Alaska, destroyed the southern 300 m of the railway dock and claimed the life of one construction worker (Kulikov *et al.*, 1996). Various estimates of wave heights range from 3 m at the ore dock to 11 m at the ferry dock (Fig. 1). The railway dock was under construction that involved deposition of a large external load of rip-rap and fill along the shoreline around one month after an important flood of the Skagway river. About 30 minutes following low tide, 3-10 million cubic meters of loose alluvial sediment slid down the fjord at various locations within the fjord inlet (Campbell, 1995). No seismic activity was recorded in the Skagway region. The Skagway harbor resonance characteristics and tide gauge record have been studied by Kulikov *et al*. (1996) and Raichlen *et al*. (1996). According to Yehle and Lemke (1972), a similar landslide occurred at the end of the railway dock in 1966. Factors that may have contributed to failure include an exceptionally low tide, recent rip-rap overburden, pile removal operations, artesian water flow through the adjacent mountain, and recent sedimentation from the Skagway river. Most spontaneous underwater landslides in fjords are associated with low, low tides (Bjerrum, 1971; Murty, 1979). Given the complex nature of failure plane nucleation, it is fundamentally impossible to ascribe mass failure to any single forcing mechanism, because local failure nuclei may have no clear connection with any global estimate of failure mechanisms, and because the entire complex of mass failures is spatially and temporally distributed.

The Skagway river delta is comprised of, and fjord walls covered with, glacial outwash either from direct emplacement or from sedimentation. This silty sediment is often sensitive to shear waves and can experience an almost total loss of shear strength when disturbed (Bardet, 1997). Therefore, we can expect nearly frictionless underwater slides that are able to trigger further landsliding by undercutting slopes or by retrogressive failure (Bjerrum, 1971). To simplify this problem considerably, we consider the tsunami amplitudes of three underwater slides in isolation that may be associated with this event: Slide A along the front of the Skagway river delta, Slide B southwest of the railway dock, and Slide C at the railway dock (Table 1). We believe that either Slide A or Slide B failed first, although the order does not particularly matter because either one could have triggered the other. The important observation is that retrogressive failure from one or the other slide led up the fjord floor to Slide C (Campbell, 1995; Plafker *et al*., 2000). Table 1 indicates that the majority of wave generation may have occurred around the shallow Slide C. The analyses in Table 1 are understood to provide a *relative* comparison between tsunami generation by the three slides considered solely in isolation. All of these potential slides generated dispersive waves within the fjord.

An even more important observation is a possible coupling between the tsunami phase speed near the shoreline and the speed of retrogressive failure, which is commonly assumed to be around 10 m/s (Bjerrum, 1971). The depression waves generated above Slides A and B will travel towards shore and propagate as an edge wave along the shoreline. The local reduction in sea level associated with the leading depression wave can induce further retrogressive failure. This failure will in turn contribute to wave generation. When these two components (wave celerity and retrogressive failure) operate at the same speed, a feedback loop is established that allows the depression wave to build while it travels towards shore or along the shoreline. The depression wave would be immediately followed by an elevation wave, which was apparently observed by eyewitnesses coming towards the railway dock and traveling northeast along the shoreline. Regardless of these dynamical and spatial complexities, the characteristic tsunami amplitude for Slide C is similar to the 9 m wave amplitude estimated from eyewitness accounts of vertical barge motion next to the remaining portion of the railway dock.

The 1999 Izmit Bay Tsunami

The M_w = 7.4 Kocaeli earthquake of Aug. 17, 1999 generated a deadly tsunami within Izmit Bay (Altinok *et al*., 1999, Yalçiner *et al*., 1999). Izmit Bay has important strike-slip faults, part of the North Anatolian Fault Zone, more or less parallel to the northern and southern shorelines (Altinok *et al*., 1999). Each one of the interconnected basins constituting Izmit Bay has apparently formed by local subsidence, as could be expected from bathymetry alone. It is well known that subsidence naturally occurs near the end of strike-slip faults, and the vertical coseismic displacement can be compounded at step-overs where slip ends along one fault and resumes along a nearby parallel fault. Localized subsidence at step-overs can also form secondary normal faults to accommodate vertical displacement near the deepest part of a basin (e.g., Altinok *et al*., 1999). We interpret the published seismic lines traversing Izmit Bay as supporting our description of subsidence (e.g., Yalçiner *et al*., 1999). There are therefore several different sources of potential tsunami generation within Izmit Bay: a subsiding block bounded by normal faults near the middle of a basin, and strike-slip faults that can serve as control faults for submarine mass failure near the northern and southern shorelines (Watts, 2001). Given the magnitude of the main shock, we believe that it is reasonable to expect all of these tsunami generation mechanisms to be present at the same time. Eyewitness observations of tsunami activity appear to validate this conjecture.

Yalçiner *et al*. (1999) report on observed leading depression waves along the northern and southern shores of Izmit Bay that were experienced almost immediately after the main shock. According to our geological interpretation, this tsunami activity suggests submarine mass failure near both shorelines. A second wave of tsunami attack is reported by Yalçiner *et al*. (1999) around five minutes after the main shock which we attribute to subsidence at the presumed step-over. We believe that shoreline subsidence reported at the town of Degirmendere may in fact be direct evidence of an underwater slump. A strike-slip control fault runs along the shoreline of the town of Degirmendere (Altinok *et al*., 1999), where significant parts of the waterfront subsided up to 20 m and experienced immediate tsunami attack of at least 2.5 m above sea level (Yalçiner *et al*., 1999). Our conjecture is supported by the captain of a fishing vessel who reported his boat being lifted at least 10 m while riding the crest of the tsunami almost immediately after the main shock (Yalçiner *et al.*, 1999). Armed with this geological and observational information, we examine the possibility that the waterfront at Degirmendere experienced an underwater slump that generated a local tsunami. We adopt a common rule of thumb and assume that slumping extends from the headwall near the shoreline down to the toe of the slope (Turner and Schuster, 1996; Bardet, 1997).

From bathymetry data for Izmit Bay, we find a slope length $b = 5$ km, a mean slope $\theta = 5^\circ$, and a mean initial submergence $d = 0.5\ b \sin\theta = 218$ m off Degirmendere. We now invoke Eqs. (8) and (11) to estimate a slump thickness $T \approx 500$ m and a slump width $w \approx 5$ km, where only part of the assumed slump headwall is exposed along the waterfront. Vertical subsidence of 20 m suggests a distance of slump motion of approximately $2s_o \approx 230$ m from the sine of slope inclination. With a radius of curvature $R \approx 6.3$ km estimated from (2), we calculate a rotational displacement of $\Delta\phi \approx 0.036$ radians from (3). The small angular displacement may be indicative of strong ground motion near the epicenter of the earthquake forcing slump motion, rather than weak sediment or pressurized water. We assume a specific density of $\gamma = 1.85$ and obtain an initial acceleration $a_o \approx 0.053$ m/s^2, a maximum velocity $u_{max} \approx 2.4$ m/s, a characteristic distance of motion $s_o \approx 115$ m, and a characteristic time of motion $t_o \approx 47$ s. This characteristic time of motion corresponds roughly to the duration of sea withdrawal immediately following the earthquake (Altinok *et al.*, 1999). The characteristic wavelength is $\lambda_o \approx 2.2$ km and leads to a 3D amplitude factor of 0.69. The characteristic tsunami amplitude above the slump is $\eta_{3d} \approx 8.2$ m, where the ratio $d/b = 0.044 < 0.06$ demonstrates that the tsunami amplitude calculation requires extrapolation. We note that there is significant potential error in most of the independent parameters given here and that this characteristic tsunami amplitude should be interpreted only in an order of magnitude sense. While much better characterization of any potential slump is needed to refine the calculations made here, we have shown that the slump hypothesis is consistent with the available observations.

The 1946 Unimak, Alaska Tsunami

The April 1, 1946 Alaskan tsunami remains an enigma for several important reasons. First, the earthquake source mechanism has undergone many revisions over time that have tended to increase the main shock magnitude from around $M \approx 7$ to $M \approx 8$ (Johnson and Satake, 1997). These revisions may have been made to help explain the devastating transoceanic tsunami that results from the event, assuming an earthquake source. Second, Mader and Curtis (1991) needed vertical coseismic displacement of 20 m to explain the large runups in Hawaii. This magnitude of displacement is difficult to reconcile with current marine geology interpretations and typical seismological parameters. Third, the earthquake magnitude versus maximum runup produces the largest disparity of any tsunami during the 20th century, larger than even the 1998 Papua New Guinea catastrophe, which suggests an underwater landslide source (Fryer et al., 2002). Fourth, despite the large local and transoceanic tsunami damage, there is a very rapid drop in tsunami amplitude away from a Great Circle axis connecting Unimak Island to the Marquesas Islands and onward to Antarctica (Fryer et al., 2002). A large earthquake can produce far-field wave energy directivity, but only an underwater landslide can produce both near-field and far-field wave energy directivity (Iwasaki, 1997; Watts, 2001). Fifth, an apparent underwater landslide scar exists in the suspected region of tsunami generation (Fryer et al., 2002). We show that many of these tsunami features can be explained by our order of magnitude analyses.

The starting point in our analysis is the measured tsunami period of 15 minutes, which should be indicative of a massive earthquake in the 6 km deep waters of the Aleutian Trench. Because the earthquake was in fact relatively weak, we use this tsunami period to invert for either a slide length $b \approx 40$ km (given a mean incline of $\theta = 4.3°$), or a slump radius of curvature $R \approx 2347$ km, both assuming a specific density of $\gamma = 1.85$. Clearly, the underwater slide hypothesis is the more reasonable of these two end members. This conjecture agrees with the key geological fact that much of the continental shelf should be covered by glacial till that fails as long slides along weak layers (Syvitski and Hutton, 2002). We estimate a slide thickness $T \approx 400$ m from (7) that is consistent with bathymetric and backscatter data (Fryer *et al.*, 2002). This same data suggests a slide width $w \approx 25$ km. We calculate an initial acceleration $a_o \approx 0.22$ m/s^2, a terminal velocity $u_t \approx 199$ m/s, and a characteristic distance of motion $s_o \approx 179$ km. Watts *et al.* (2002b) showed that most underwater slides only reach a maximum velocity of $0.43u_t$ at the bottom of a slope, which yields $u_{max} \approx 86$ m/s in this case, well within the range of expected slide velocities (Kuenen, 1952). Assuming that the headwall intersects the continental shelf at $h = 100$ m (Fryer *et al.*, 2002), we find a mean initial depth $d = 1.6$ km for the slide. The characteristic wavelength is $\lambda_o \approx 113$ km and leads to a 3D amplitude factor of 0.18. This tsunami would propagate as shallow water waves across the Pacific Basin. The characteristic tsunami amplitude above the slide is $\eta_{3d} \approx 32$ m where the ratio $d/b = 0.04 < 0.06$ involves some tsunami amplitude extrapolation. Once again, we find that the characteristic tsunami amplitude agrees with the necessary runup above sea level to account for lighthouse destruction at Scotch Cap, which is more or less in line with the axis of failure. The characteristic tsunami wavelength on the shelf is $\lambda_o \sqrt{h / d} \approx 28$ km which gives rise to an Ursell parameter U $\approx 25{,}000$ that indicates nonlinear, shallow water waves. We therefore hypothesize that Scotch Cap lighthouse may have been attacked by a bore traversing the continental shelf.

The Ontong Java Plateau Slide

One of the largest mass failures on earth exists on the northeastern margin of the Ontong Java Plateau. The landslide scar, Nukumanu Canyon, extends from near Nukumanu Island at the crest of the plateau down into the Nauru Basin, a total vertical drop of 2 km over a horizontal distance of over 500 km. The canyon is clearly visible on any modern map of the Pacific Ocean, almost regardless of scale (Fig. 1). The feature was identified as a landslide by Kroenke (1972). Seismic reflection profiles across the canyon show truncated sedimentary layers, precipitous channel walls, and isolated buttes within the channel (Kroenke, 1972; Berger et al., 1977). Profiles along the channel and out into the Nauru Basin show debris flows and turbidites (Kroenke et al., 1971; Berger et al., 1977). Cores from the axis of the canyon recovered carbonates well below the carbonate compensation depth, and contained shallow-water foraminifera, confirming a sudden, catastrophic origin (Berger and Johnson, 1976). Taken together, the data suggest a single mass failure, though the age of the event has yet to be determined. We study the Nukumanu Canyon event in order to illustrate the sometimes surprising consequences of tsunami generation by underwater landslides. Based on the scar dimensions, we estimate an initial length $b = 200$ km, an initial thickness $T = 1$ km, a width $w = 100$ km, a mean initial depth $d = 3.3$ km, and a mean slope of $\theta = 0.5^\circ$ that are reasonably consistent with Eqs. (7) and (10), and therefore indicative of an underwater slide. This event could reach a volume of 16,000 km^3 if it were indeed a single mass failure.

We assume a specific density of $\gamma = 1.85$ and calculate an initial acceleration $a_o \approx 0.026$ m/s^2, a terminal velocity $u_t \approx 152$ m/s, a characteristic distance of motion $s_o \approx 896$ km, and a characteristic time of motion $t_o \approx 5915$ s. We expect a maximum velocity of $0.43u_t = 65$ m/s for this slide, due largely to the extreme length of this potential event. The characteristic distance of motion has the same order of magnitude as the observed deposit length. The characteristic wavelength is $\lambda_o \approx 1064$ km and leads to a 3D amplitude factor of 0.086. The characteristic tsunami amplitude above the slide is $\eta_{3d} \approx 8.2$ m although the ratio d/b = 0.0165 < 0.06 raises some doubt as to the accuracy of the extrapolation. Nevertheless, the tsunami amplitude calculated here should be an upper bound on the potential tsunami amplitude. The singularity in the tsunami amplitude equation as the initial depth vanishes is spurious, in part because the near-field wave amplitude will eventually saturate to a maximum of around 0.86 h (Mei, 1983). The tsunami described here clearly gives rise to linear, nondispersive, shallow water waves that should traverse the Pacific Basin. However, the small angle of inclination and large wavelength keep the tsunami amplitude small despite the massive landslide size. Consequently, we do not expect any discernible paleo-tsunami deposits for this potential event given a maximum far-field runup approximated by the characteristic tsunami amplitude.

THE CORRESPONDENCE PRINCIPLE

Our analyses have usually focused on tsunami generation near the source rather than the propagation and runup of local tsunamis. When first testing the value of analytical expressions for tsunami generation, we observed a correspondence between the characteristic tsunami amplitude at the source and the maximum runup above sea level along the nearest shoreline. The observed correspondence helped justify our choice to study exclusively tsunami generation. Hence, tsunami generation estimates provided an immediate payback in the form of maximum runup estimates with a similar degree of approximation. We therefore propose a Correspondence Principle that states:

A characteristic tsunami amplitude at generation can be found that will approximate the maximum runup of local tsunamis generated by underwater landslides.

This correspondence arises because wavefront spreading during propagation is compensated for by shoaling and refractive focusing. The spreading reduces amplitude whereas the shoaling and focusing rebuild amplitude. The principle is not intended to replace numerical simulations of tsunami propagation and inundation, especially because the principle does not indicate where maximum runup will occur. Nevertheless, the effectiveness of the principle is evident from available case studies and provides an immediate regional assessment of local tsunami hazard.

CONCLUSIONS

Our results indicate that tsunami source characterization is the single most important research activity related to landslide tsunamis and that source characterization is intimately linked to the marine geology setting. We explain the role played by the landslide initial acceleration in tsunami generation. We show that the initial acceleration is the only center of mass motion experienced during tsunami generation and demonstrate the connection of initial acceleration to our scaling analyses. These scaling analyses indicate that most underwater landslide parameters with dimension of length can be related to the landslide length. We show that underwater landslide width can have an important impact on the 3D characteristic tsunami amplitude. We suggest that slumps may be more efficient tsunami sources than slides. We solve an apparent paradox in slump center of mass motion whereby the distance traveled is proportional to the shear strength. The distance traveled is instead expressed by a departure in shear strength from being proportional to the overburden. We demonstrate that rundown and runup can be scaled with the characteristic tsunami amplitude, thereby proving the fundamental and global utility of a tsunami amplitude within the generation region. Our case studies of five potential landslide tsunamis show that our analyses can describe many tsunami features, in some cases reproducing important eyewitness accounts. We anticipate that the characteristic tsunami amplitude would be a reasonable representation of maximum runup in a three-dimensional geometry. We therefore propose the Correspondence Principle as an extension of the case studies presented here.

ACKNOWLEDGMENTS

The authors wish to acknowledge Applied Fluids Engineering, Inc. for substantial and extended support of this research. Partial support for this work was provided by the FEMA under grant DR-1008-9004 made to Costas Synolakis at USC, and by the NSF under research grant CMS-0100223 made to STG at URI. Slava Gusiakov and Mike Blackford provided data regarding the frequency and intensity of tsunamigenic underwater landslides. The authors benefited from discussions with Jose Borrero, George Plafker, Costas Synolakis, and Ahmet Yalçiner. DRT publishes by permission of the British Geological Survey, Natural Environment Research Council, United Kingdom.

APPENDIX I. REFERENCES

Altinok, Y., Alpar, B., Ersoy, S., and Yalçiner, A. C. (1999). "Tsunami generation of the Kocaeli Earthquake (August 17th 1999) in Izmit Bay; coastal observations, bathymetry and seismic data." *Turkish J. Marine Sciences*, 5(3),131-148.

Bardet, J.-P. (1997). *Experimental Soil Mechanics*. Prentice Hall, Upper Saddle River, New Jersey.

Berger, W. H., and Johnson, T. C. (1976). "Deep-sea carbonates: Dissolution and mass wasting on Ontong Java Plateau." *Science*, 192, 785-787.

Berger, W. H., Johnson, T. C., and Hamilton, E. L. (1977). "Sedimentation on Ontong Java Plateau: Observations on a classic 'carbonate monitor'." In: E. R. Andersen and A. Malahoff (Eds.) *The fate of fossil fuel CO2 in the oceans*, Plenum Press, New York, 543-567.

Bjerrum, L. (1971). "Subaqueous slope failures in Norwegian fjords." *Nor. Geotech. Inst. Bull.*, 88, 1-8.

Campbell, B. A. (1995). "Report of a seafloor instability at Skagway, Alaska, November 3, 1994." *Campbell and Associates*, 14104 Hancock Drive, Anchorage, Alaska, 99515.

Caplan-Auerbach, J., Fox, C. G., and Duennebier, F. K. (2001). "Hydroacoustic detection of submarine landslides on Kilauea volcano." *Geophys. Res. Lett.*, 28(9), 1811-1813.

Edgers, L., and Karlsrud, K. (1982). "Soil flows generated by submarine slides: Case studies and consequences." *Nor. Geotech. Inst. Bull.*, 143, 1-11.

Fryer, G. J., Watts, P., and Pratson, L. F. (2002). "Source of the great tsunami of 1 April 1946: A landslide in the upper Aleutian forearc." *Marine Geology*, submitted.

Geist, E. L. (1998). "Local tsunamis and earthquake source parameters." *Adv. in Geophys.*, 39, 117-209.

Hammack, J. L. (1973). "A note on tsunamis: Their generation and propagation in an ocean of uniform depth." *J. Fluid Mech.*, 60, 769-799.

Hampton, M. A., Lee, H. J., and Locat, J. (1996). "Submarine landslides." *Rev. Geophys.*, 34(1), 33-59.

Iwasaki, S. (1997). "The wave forms and directivity of a tsunami generated by an earthquake and a landslide." *Sci. Tsunami Hazards*, 15, 23-40.

Jiang, L., and LeBlond, P. H. (1992). "The coupling of a submarine slide and the surface waves which it generates." *J. Geoph. Res.*, 97(C8), 12731-12744.

Johnson, J. M., and Satake, K. (1997). "Estimation of seismic moment and slip distribution of the April 1, 1946, Aleutian tsunami earthquake." *J. Geoph. Res.*, 102, 11765-11774.

Kawata, Y. and International Tsunami Survey Team members. (1999). "Tsunami in Papua New Guinea was intense as first thought." *Eos, Trans. Am. Geophys. Union*, 80(9), 101.

Kramer, S. L. (1996). *Geotechnical earthquake engineering*. Prentice Hall, Upper Saddle River, NJ.

Kroenke, L., Moberly, R., Winterer, E. L., and Heath, G. R. (1971). "Lithologic interpretation of continuous reflection profiling, Deep Sea Drilling Project Leg 7." *Init. Repts. Deep Sea Drilling Proj.*, 7, 1161-1226.

Kroenke, L. W. (1972). "Geology of the Ontong Java Plateau," PhD thesis, University of Hawaii, Honolulu, HI.

Kuenen, Ph. H. (1952). "Estimated size of the Grand Banks turbidity current." *Am. J. Science*, 250, 874-884.

Kulikov, E. A., Rabinovich, A. B., Thomson, R. E., and Bornhold, B. D. (1996). "The landslide tsunami of November 3, 1994, Skagway harbor, Alaska." *J. Geoph. Res.*, 101(C3), 6609-6615.

Mader, C. L., and Curtis, G. (1991). "Modeling Hilo, Hawaii tsunami inundation." *Sci. Tsunami Hazards*, 9, 85-94.

Martel, S. J. (2002). "Submarine landslides as a shear fracture phenomenon." In: P. Watts, C. E. Synolakis, and J. P. Bardet (eds), Prediction of underwater landslide hazards, Swets & Zeitlinger, Rotterdam, The Netherlands.

Matsuyama, M., Walsh, J. P., and Yeh, H. (1999). "The effect of bathymetry on tsunami characteristics at Sissano Lagoon, Papua New Guinea." *Geophys. Res. Lett.*, 26, 3513-3516.

McAdoo, B. G., Pratson, L. F., and Orange, D. L. (2000). "Submarine landslide geomorphology, US continental slope." *Marine Geol.*, 169, 103-136.

Mei, C. C. (1983). *The applied dynamics of ocean surface waves*. World Scientific, Teaneck, N.J.

Murty, T. S. (1979). "Submarine slide-generated water waves in Kitimat Inlet, British Columbia." *J. Geoph. Res.*, 84(C12), 7777-7779.

Pelinovsky, E., and Poplavsky, A. (1996). "Simplified model of tsunami generation by submarine landslide." *Phys. Chem. Earth*, 21(12), 13-17.

Plafker, G., Kachadoorian, R., Eckel, E. B., and Mayo, L. R. (1969). "The Alaska earthquake March 27, 1964: Various communities." U.S. Geol. Surv. Prof. Paper 542-G, U.S., Dept. of Interior, Washington, DC.

Plafker, G., Greene, H. G., Maher, N., and Synolakis, C. E. (2000). "Mechanism of the November 3, 1994 submarine landslide and associated landslide-generated tsunami at Skagway, Alaska." *Eos, Trans. Am. Geophys. Union*, 81(48), f759.

Prior, D. B., and Coleman, J. M. (1979). "Submarine landslides: Geometry and nomenclature." *Z. Geomorph. N. F.*, 23(4), 415-426.

Raichlen, F., Lee, J. J., Petroff, C., and Watts, P. (1996). "The generation of waves by a landslide: Skagway, Alaska case study." *Proc., 25th Int. Conf. Coastal Engrg.*, Orlando, FA, ASCE, 1293-1300.

Schwab, W. C., Lee, H. J., Twichell, D. C. (1993). *Submarine landslides: Selected studies in the U.S. exclusive economic zone*. Bull. 2002, U.S. Geol. Surv., U.S., Dept. of Interior, Washington, DC.

Sibson, R. H. (1981). "Controls on low stress hydro-fracture dilatancy in thrust wrench and normal fault terranes." *Nature*, 289, 665-667.

Striem, H. L., and Miloh, T. (1976). "Tsunamis induced by submarine slumpings off the coast of Israel." *Int. Hydrographic Review*, 2, 41-55.

Sweet, S., and Silver, E. A. (2002). "Seismic reflection images of the source region of the 1998 Papua New Guinea tsunami." In: P. Watts, C. E. Synolakis, and J. P. Bardet (eds), Prediction of underwater landslide hazards, Swets & Zeitlinger, Rotterdam, The Netherlands.

Syvitski, J. P. M., and Hutton, E. W. H. (2002). "Failure of marine deposits and their redistribution by sediment gravity flows." In: P. Watts, C. E. Synolakis, and J. P. Bardet (eds), Prediction of underwater landslide hazards, Swets & Zeitlinger, Rotterdam, The Netherlands.

Tappin, D. R., Watts, P., McMurtry, G. M., Lafoy, Y., Matsumoto, T. (2001). The Sissano, Papua New Guinea Tsunami of July 1998 -- Offshore Evidence on the Source Mechanism. *Marine Geology*, 175, 1-23.

Tappin, D. R., and Shipboard Scientists. (1999). "Offshore surveys identify sediment slump as likely cause of devastating Papua New Guinea tsunami 1998." *Eos, Trans. Am. Geophys. Union*, 80(30), July 27, 329.

Terzaghi, K. (1956). "Varieties of submarine slope failures." *Proc., 8th Texas Conf. Soil Mech. Found. Engrg.*, 1-41.

Tinti, S., and Bortolucci, E. (2000). "Energy of water waves induced by submarine landslides." *Pure Appl. Geophys.*, 157, 281–318.

Tuck, E. O., and Hwang, L.-S. (1972). "Long wave generation on a sloping beach." *J. Fluid Mech.*, 51(3), 449-461.

Turner, A. K., and Schuster, R. L. (1996). *Landslides: Investigation and mitigation*. Special Report 247, Trans. Res. Board, National Academy Press, Washington, DC.

von Huene, R, Ranero, C. R., and Watts, P. (2002). "Tsunamigenic slope failure along the Middle America Trench in two tectonic settings." In: P. Watts, C. E. Synolakis, and J. P. Bardet (eds), Prediction of underwater landslide hazards, Swets & Zeitlinger, Rotterdam, The Netherlands.

Watts, P. (1997). "Water waves generated by underwater landslides," PhD thesis, California Inst. of Technol., Pasadena, CA.

Watts, P. (1998). "Wavemaker curves for tsunamis generated by underwater landslides." *J. Wtrwy, Port, Coast, and Oc. Engrg.*, ASCE, 124(3), 127-137.

Watts, P. (2000). "Tsunami features of solid block underwater landslides." *J. Wtrwy, Port, Coast, and Oc. Engrg.*, ASCE, 126(3), 144-152.

Watts, P., Imamura, F., and Grilli, S. T. (2000). "Comparing model simulations of three benchmark tsunami generation cases." *Sci. Tsunami Hazards*, 18(2), 107-124.

Watts, P. (2001). "Some opportunities of the landslide tsunami hypothesis." *Sci. Tsunami Hazards*, 19(3), 126-149.

Watts, P., Borrero, J. C., Tappin, D. R., Bardet, J.-P., Grilli, S. T., Synolakis, C. E. (2002a). "Novel simulation technique employed on the 1998 Papua New Guinea tsunami." Presented at the 1999 IUGG General Assembly in Birmingham, UK, and published by the first author at *www.appliedfluids.com/resume.html*.

Watts, P., Gardner, J. V., Yalçiner, A. C., Imamura, F., and Synolakis, C. E. (2002b). "Landslide tsunami scenario off Palos Verdes, California." *Natural Hazards*, in press.

Watts, P., and Borrero, J. C. (2002). "Probabilistic predictions of underwater landslides and tsunami amplitudes." In: P. Watts, C. E. Synolakis, and J. P. Bardet (eds), Prediction of underwater landslide hazards, Swets & Zeitlinger, Rotterdam, The Netherlands.

Wilson, R. C., and Keefer, D. K. (1985). *Predicting areal limits of earthquake-induced landsliding*. Prof. Paper 1360, U.S. Geol. Survey, U.S., Dept. of Interior, Washington, DC.

Yalçiner, A. C., Synolakis, C. E., Borrero, J. C., Altinok, Y., Watts, P., Imamura, F., Kuran, U., Ersoy, S., Kanoglu, U., and Tinti, S. (1999). "Tsunami generation in Izmit Bay by the 1999 Izmit Earthquake." Conference on the 1999 Kocaeli Earthquake, Istanbul Technical University Press, 217-221.

Yehle, L. A., and Lemke, R. W. (1972). "Reconnaissance engineering geology of the Skagway area, Alaska, with emphasis on evaluation of earthquake and other geological hazards." *Open File Report*, U.S., Geol. Survey.

APPENDIX II. NOTATION

The following symbols are used in this paper:

a_o	=	Initial acceleration;
b	=	Length of landslide along incline;
d	=	Initial landslide submergence;
f	=	Function;
g	=	Gravitational acceleration;
h	=	Local water depth;
k	=	Nondimensional coefficient;
M	=	Earthquake magnitude;
R	=	Correlation coefficient; radius of curvature; runup; rundown;
s	=	Position coordinate along incline;
s_o	=	Characteristic length scale of motion ($s_o=u_t^2/a_o$);
Su	=	Sediment shear strength;
t	=	Time;
T	=	Landslide thickness;
t_o	=	Characteristic time scale of motion ($t_o=u_t/a_o$);
U	=	Ursell parameter ($U=a\lambda_d^2/h^3$);
u_t	=	Landslide terminal velocity;
w	=	Width of landslide;
y	=	Width coordinate;
z	=	Depth coordinate:
$\Delta\phi$	=	Angular displacement;
γ	=	Specific density ($\gamma=\rho_b/\rho_o$);
η	=	Free surface amplitude;
λ_o	=	Characteristic near-field wavelength ($\lambda_o=t_o\sqrt{gd}$);
θ	=	Angle of the incline from horizontal;
ρ_b	=	Bulk landslide density;
ρ_o	=	Density of water;

Subscripts

2d	=	Two-dimensional;
3d	=	Three-dimensional;
b	=	Bulk;

g	=	Gravitational;
m	=	Added mass;
max	=	Maximum or upper bound;
o	=	Ambient water; characteristic; initial;
t	=	Terminal;
w	=	Moment;

TABLE 1. Skagway, Alaska Approximate Slide Quantities

Quantities	Slide A	Slide B	Slide C
γ	1.85	1.85	1.85
b (m)	600	215	180
T (m)	15	15	20
w (m)	340	390	360
d (m)	150	95	24
θ	9	22	24
a_o (m/s^2)	0.46	1.10	1.20
u_t (m/s)	35	33	31
s_o (m)	2688	963	806
t_o (s)	77	30	26
λ_o (m)	2935	904	399
η_{3d} (m)	0.16	0.59	5.9

Fig. 1: Contour plot of Skagway harbor bathymetry with 50 m contours and approximate slide and dock locations in meters with arbitrary origin

Fig. 2. Contour plot of sea floor bathymetry along the north face of the Ontong Java Plateau

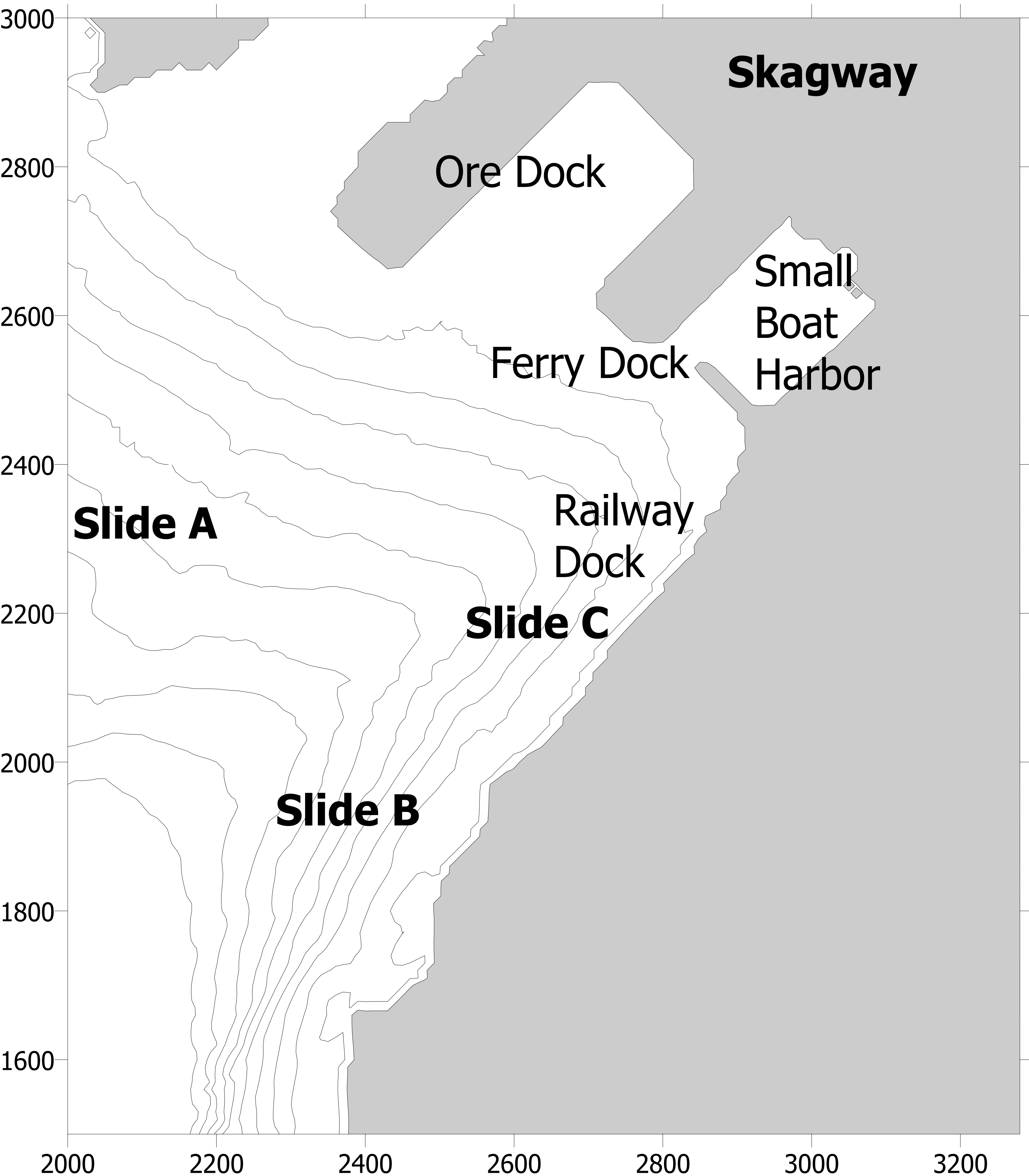
Skagway
Ore Dock
Small
Boat
Harbor
Ferry Dock
Railway
Dock
Slide A
Slide C
Slide B
3000
2800
2600
2400
2200
2000
1800
1600
2000
2200
2400
2600
2800
3000
3200

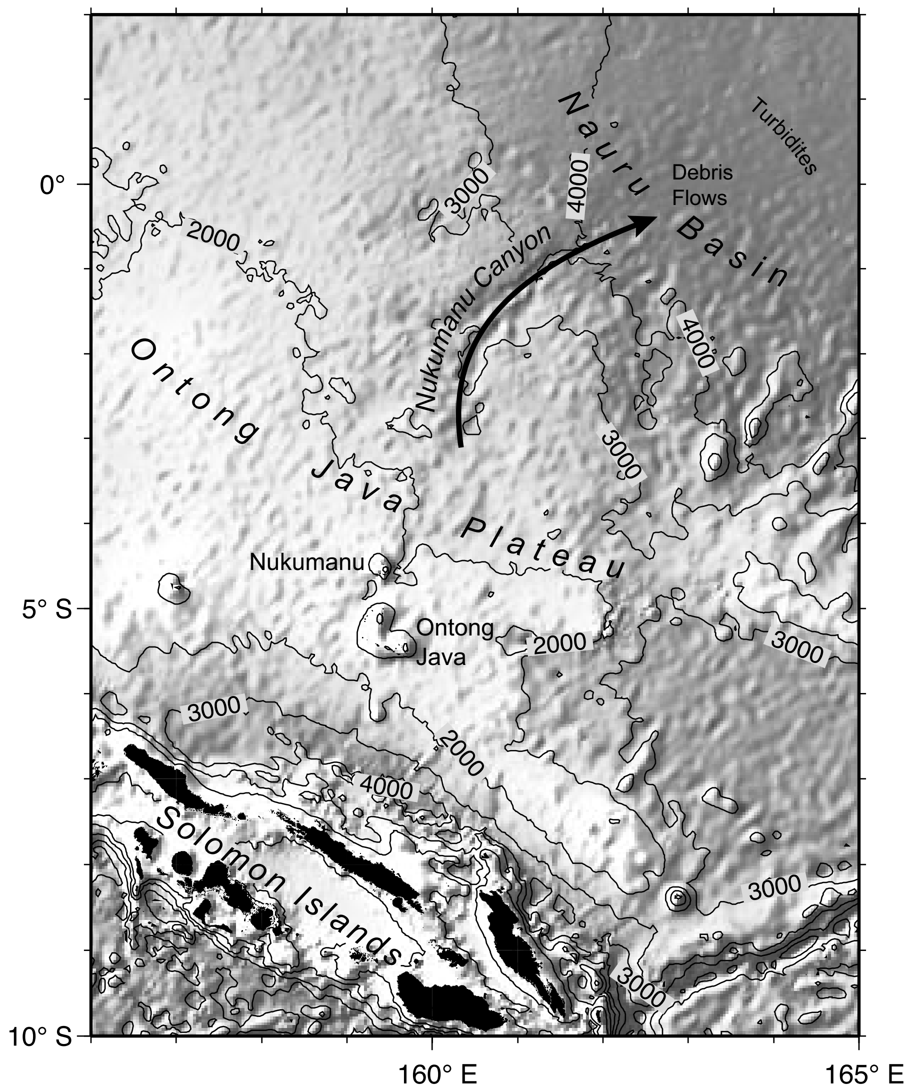

0°
5° S
10° S
160° E
165° E
Nauru Basin
Turbidites
Debris
Flows
Nukumanu Canyon
Ontong Java Plateau
Nukumanu
Ontong
Java
Solomon Islands
2000
3000
4000